Spin-dependent electron momentum densities in Cu_2MnAl studied by Compton scattering

1997 J. Phys.: Condens. Matter 9 10993

(http://iopscience.iop.org/0953-8984/9/49/017)

J. Phys.: Condens. Matter **9** (1997) 10993–11005. Printed in the UK PII: S0953-8984(97)85659-7

Spin-dependent electron momentum densities in Cu_2MnAl studied by Compton scattering

E Żukowski†, A Andrejczuk†, L Dobrzyñski†*, M J Cooper‡, M A G Dixon‡, S Gardelis‡, P K Lawson‡, T Buslaps§, S Kaprzyk‖, K-U Neumann¶ and K R A Ziebeck¶

† Institute of Physics, Warsaw University Branch, 15-424 Bialystok, Poland
‡ Department of Physics, University of Warwick, Coventry CV4 7AL, UK
§ ESRF, F-38043 Grenoble Cédex, France
‖ University of Mining and Metallurgy, 30-059 Kraków, Poland
¶ Department of Physics, Loughborough University, Leicestershire LE11 3TU, UK
* Soltan Institute for Nuclear Studies, 05–4000 Otwock-Swierk, Poland

Received 2 July 1997, in final form 16 September 1997

Abstract. The spin density in the Heusler alloy Cu_2MnAl, has been studied in a Compton scattering experiment with 92 keV circularly polarized synchrotron radiation on the high-energy beamline at ESRF. The conduction electrons were found to have a negative spin polarization of 0.4 μ_B which is at variance with the deduction of a positive moment from earlier neutron data; neither was any evidence found for a 3d spin moment on the copper site. The spin moment on the Mn site at room temperature was determined as 3.25 μ_B, which is in agreement with neutron data. The spin-dependent Compton profiles for the [100], [110] and [111] directions, reported here, show anisotropy in the momentum density which is in good agreement with new KKR calculations based on a ferromagnetic ground state. By combining charge- and spin-dependent Compton data the momentum space anisotropies in the majority and minority bands have been analysed. Both the majority and minority spin densities are anisotropic.

1. Introduction

Heusler alloys are ternary intermetallic compounds with stoichiometric composition X_2YZ, where X can be a 3d, 4d or 5d element (e.g. Fe, Co, Ni, Cu, Zn, Ru, Rb, ...); Y a rare earth or, for example, Ti, V, Mn, Y, Zr, Nb, and Z is, for example, Al, Si, Ga, Ge, As, In or Sn. They have either the $L2_1$, DO_3 or B2 structure. Heusler alloys are interesting magnetic systems because they possess localized magnetic moments although they are all metallic. In some cases, ferromagnetic order is achieved even though none of the constituent elements is itself a ferromagnet; the majority of these are soft ferromagnets. The prototype Heusler alloy is Cu_2MnAl, which has the $L2_1$ structure with the unit cell consisting of four interpenetrating face-centred cubic sub-lattices. In the standard terminology for the sites, see *Landolt–Börnstein* [1], the Cu atoms occupy B and D sites, and Mn and Al atoms go preferentially to C and A sites, respectively. The Curie temperature, lattice constant and saturation moment are 603 K, 0.5949 nm and 4.12 μ_B, respectively [1]. Extensive investigations of the magnetic, electrical and structural properties of Cu_2MnAl have also been carried out [2–6]. The formation and coupling of the magnetic moments in Mn-related Heusler alloys are still the subject of theoretical and experimental studies. From early neutron spin wave scattering experiments performed on Pd_2MnSn, Ni_2MnSn and Cu_2MnAl

0953-8984/97/4910993+13$19.50

samples [7–9] it was concluded that the 3d electrons are well localized on the Mn atoms (the results of Noda and Ishikawa [7], for example, were analysed using a Hamiltonian where only the Mn atoms have a localized moment) and the interactions in the Heusler alloys are long range, extending to more than eight neighbours. These large-distance Mn–Mn interactions are explained by an s–d interaction of the RKKY type.

A number of theoretical calculations of electronic structure and magnetic moment formation in Heusler alloys [10–14], accompanied the early experimental findings. In particular Williams *et al* [10] and Kübler *et al* [11], examining the self-consistent spin-polarized energy band calculations, concluded that there is no direct interaction between the d states on Mn atoms and argued for delocalized d electrons in a common band formed by the Mn and Cu atoms. In their picture hybridization of the Al p and Mn d states mediated the covalent interactions between the Mn atoms. A more general theoretical discussion of the ferromagnetic moment formation in transition-metal alloys including itinerant ferromagnetism was presented by Kübler [12] who found that the role of the X atom (Cu in this sample) in Heusler alloys is limited to the determination of the lattice constant, except when X is either Co or Ni, in which case there is additional induced magnetization. The KKR calculations of electronic and magnetic properties of such alloys were presented by Fujii *et al* [13] and a similar approach to Co–Ni Heusler alloys, with details of band structure calculations, has been published by Tobola *et al* [14]. Williams *et al* [10] concluded that there were no spin-down 3d electrons on the manganese site, leaving a localized moment on the Mn site. These theoretical predictions have been recently examined experimentally by ultraviolet photoemission spectroscopy [15]. The measured spectra revealed the Mn 3d contribution across the full width of the valence band and a strong enhancement at the energies which might be mainly attributed to the contributions from the Cu d bands which are not completely full. However, the predicted peak, related to the contribution from both Cu and Mn 3d states, was not observed.

The magnetizations on the different sites were determined by Rakhecha *et al* [16] two decades ago, using the polarized neutron technique to study the magnetic form factor of $Cu_{2.08}Mn_{0.86}Al_{1.06}$ at room temperature; the authors presented more extensive polarized neutron measurements than those reported previously [17, 18]. The magnetic moment of the Mn atom was determined as 3.20(6) μ_B. This agreed well with an earlier value, also obtained by neutron scattering, by Takata [18]. An upper limit of 0.02(3) μ_B for the negative magnetic moment at the Cu site was predicted by Rakhecha *et al* By combining these results with magnetization data a moment of $+0.17$ μ_B was attributed to the conduction electrons; this positive spin polarization is surprising in the light of early theoretical calculations of Ishida *et al* [19] who predicted a moment of -0.046 μ_B at the Al sites, and a positive moment $+0.073$ μ_B at the Cu sites. It is opposite to what is normally found in most 3d transition metal and alloy ferromagnets and motivated the present Compton scattering investigation. No significant asphericity of the Mn spin density was observed in these earlier experiments and the results were very well accounted for by the calculated spherically symmetric Mn^{2+} free ion form factor [20] for all observed reflections. A similar conclusion was reached by Ishikawa *et al* for Pd_2MnSn [21]. However, in this case the magnetic moment of Mn was found to be 4.26(10) μ_B, which is significantly larger than in Cu_2MnAl, and the conduction electron polarization was negative.

The computation of the Compton profiles has been performed using a spin-polarized version of multiple-scattering theory based upon the Korringa–Kohn–Rostoker (KKR) band technique. First the effective one-electron potential was constructed within the density functional framework, using the local spin density approximation (LSD). Next the Green function was constructed and converted to momentum space. The spin-resolved momentum

densities were calculated at $196 \times 48 \times 1837$ momentum values, i.e. at 196 k-points in the irreducible segment (1/48th) of the Brillouin zone and for 1837 reciprocal lattice vectors. The band electron Compton profiles for a number of crystallographic directions were then determined up to $p_z = 6.8$ au, which corresponds to the maximum reciprocal lattice vector in the calculation: in addition the core electron momentum density was calculated in the KKR scheme up to 13 au (electron momenta, p_z, are normally quoted in atomic units, au, where $\overline{h} = m = e = 1$ and $c = 137$, then 1 au of momentum $= 1.99 \times 10^{-24}$ kg m s^{-1}). The model produced a zero-temperature spin moment of 3.4 μ_B.

Compton scattering is an incoherent process, therefore the method can only be applied to materials with a net moment, i.e. ferro- or ferri-magnets. This is precisely the class of materials that have to date been neglected in magnetic diffraction studies in favour of antiferromagnets because of the relative difficulty of separating the superimposed magnetic and charge peaks in the former. Comprehensive reviews of Compton scattering related to both charge and magnetization densities can be found in [23–25]. Briefly, when unpolarized, or linearly polarized radiation is used the spectrum of the inelastically scattered radiation can be interpreted, within an impulse approximation, in terms of the projection of the electron momentum distribution, $n(\boldsymbol{p})$, along the scattering vector. This quantity is referred to as the Compton profile and usually denoted $J(p_z)$ where the z direction is parallel to the scattering vector.

$$J(p_z) = \iint [n(\boldsymbol{p})\uparrow + n(\boldsymbol{p})\downarrow] \, \mathrm{d}p_x \, \mathrm{d}p_y. \tag{1}$$

In the above equation the momentum density distribution, $n(\boldsymbol{p})$, has been split into spin up, $n(\boldsymbol{p})\uparrow$, and spin down, $n(\boldsymbol{p})\downarrow$, components. The momentum space wavefunctions, from which the density distributions are formed, are simply Fourier transforms of their more familiar position space counterparts. The measurements of $J(p_z)$ discussed later include those made with an unpolarized ^{137}Cs radioisotope source in one of our laboratories [26] as well as with circularly polarized synchrotron radiation.

If circularly polarized radiation is used there is a coupling between the charge and spin scattering which produces a term depending on the spin density. The magnetic Compton profile $J_{mag}(p_z)$, which can then be deduced from the scattering cross-section, is defined as:

$$J_{mag}(p_z) = \iint [n(\boldsymbol{p})\uparrow - n(\boldsymbol{p})\downarrow] \, \mathrm{d}p_x \, \mathrm{d}p_y. \tag{2}$$

Experimentally it is obtained by reversing the direction of the sample magnetization and forming the difference between the *spin up* and *spin down* signals, thereby eliminating the charge scattering, which is unaffected by the field direction [27, 28]. The magnetic scattering is a small fraction of the charge scattering, amounting to 1–2% of the latter in the case of an Fe sample. In magnetic Compton scattering experiments carried out within the impulse approximation it is the spin magnetization that is measured: the orbital contribution is absent, a point that has been the subject of considerable experimental and theoretical investigation [24, 25, 29–32]. The term 'magnetic Compton profile' is now common currency although spin-dependent profile would be a more appropriate nomenclature. The area under the Compton profile, $J(p_z)$, integrated over all momenta, is just equal to the total number of electrons whereas the area under the magnetic Compton profile is numerically equal to the spin moment in Bohr magnetons, μ_B. Thus measurements can be calibrated by measuring the magnetic Compton profile of ferromagnetic iron, for example, which has a well known spin moment. Although the observed line contains contributions from all electrons with unpaired spins the site-dependent spin moments can generally be deduced

because the momentum density distributions, which are associated with each site and with the diffuse component, are significantly different and this has been exploited in the case of a number of rare earth ferromagnetic compounds [33, 34] and most recently in $CeFe_2$ [35], UFe_2 [36] and $SmCo_5$ [37].

2. Experimental procedure

The measurements were carried out on the high-energy beamline at the ESRF in Grenoble. The technique used on this particular beamline has been fully described recently in a paper by McCarthy *et al* [38] to which the reader is referred for further details. A synchrotron is a natural source of circularly polarized radiation. In the orbital plane the radiation is completely polarized in that plane, but out of the orbital plane a perpendicularly polarized component arises, the radiation is elliptically polarized and the 'inclined view method' has been used from the earliest synchrotron studies of magnetic Compton scattering [39]. Since the two linear components parallel and perpendicular to the orbital plane are in quadrature, a simple definition of the degree of circular polarization, P_c, is:

$$P_c = \frac{2\sqrt{(I_\parallel I_\perp)}}{(I_\parallel + I_\perp)} \tag{3}$$

where $I_\parallel$ and $I_\perp$ are the intensities of the parallel and perpendicular components.

In practice a beam with a degree of circular polarization of approximately 50% was extracted from an asymmetric multipole wiggler which has a critical energy of 43 keV by viewing the source at an angle of 10–60 μrad to the orbital plane (i.e. 0.7–4.2 mm above the orbital plane at the sample position). This wedge of radiation is chosen in order to maximize the ratio of the small magnetic signal, which is proportional to $P_c I$ to the statistical noise of the Compton (charge) scattering, which is proportional to $\sqrt{I}$ and threatens to obscure the former. This procedure produces a 'figure of merit' of $P_c\sqrt{I}$, where I is the flux incident upon the sample [28, 38, 39] that has to be maximized experimentally.

The beam was monochromated by an Si(220) bent crystal in Bragg geometry. The monochromator was oriented so as to deliver photons with energies 46 keV, 92 keV, 138 keV etc. The first harmonic at 92 keV was selected, the fundamental being effectively removed from the beam by a copper attenuator. The scattering angle was 167.3° ($\pm 0.3^\circ$), giving a Compton peak at 67.85 keV. Compton peaks at 90.0 and 107.4 keV from higher harmonics of the monochromator at 138 and 184 keV were measurable but produced minimal interference. The single-crystal sample was a rectangular column with dimensions 3 mm $\times$ 2.5 mm $\times$ 20 mm grown along [110], one face being perpendicular to [111]. The measurements were carried out at room temperature, which is approximately half the Curie temperature, because no low-temperature facility was available at the time and the previous neutron measurements [16] with which these data are compared were also performed at room temperature. The magnetization of the sample was measured on a magnetic balance and a magnetometer at fields up to 1.3 T which is somewhat higher than the field of 0.98 T achieved in the Compton study, but either field is sufficient to saturate the magnetization.

The Compton profiles at given directions were measured in reflection geometry. Other crystallographic directions ([110] and [100]) were aligned with the scattering vector by rotation of the sample by -35° and $+55^\circ$ with respect to the [111] position. A beam 0.3–0.5 mm wide and 4 mm high was incident upon the sample. One novel feature of this experiment was the use of a rotating permanent magnet to provide a reversible field of 0.98 T. This device, which was made by Magnetic Solutions, Dublin, consists of two Halbach cylinders of NdFeB permanent magnet segments, forming a magnetic circuit that

produces a net horizontal field, across a diameter of the cylinder. The two cylinders, which would otherwise rotate to align their moments antiparallel and crash together, are held apart vertically by 5 mm and clamped in the parallel field position in a rigid holder to produce 0.98 T with a uniformity of better than 2% at the beam position on the sample. The geometry is shown in figure 1. Compared with the electromagnets used earlier it has the advantage of providing a higher magnetic field (twice as large) in a gap that can accommodate a cryostat and allowing access at virtually any scattering angle in the horizontal plane. In particular back-scattering geometries are not impeded as they would be by the poles and coils of a conventional electromagnet. The latter point is particularly important because the momentum space resolution of a Compton scattering experiment improves towards back scattering and is less degraded by the divergence of the incident and scattered beams. The field was reversed by rotating the magnet every 30 seconds through 180° with a computer-controlled pneumatic drive. It can be rotated in less than 1 s, therefore the sample has to be held rigidly to resist the torques that arise when the magnet rotates.

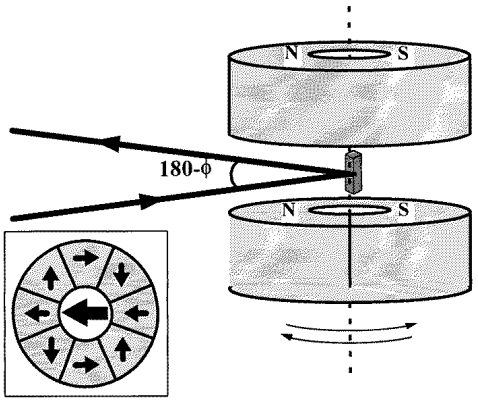

Figure 1. The scattering geometry using the rotating permanent magnet. The sketch shows an exploded perspective view of the NdFeB magnet. The upper and lower Halbach cylinders have an outer diameter of 160 mm, a bore of 45 mm and a thickness of 55 mm; in reality they are held apart by 5 mm only vertically. The inset shows the orientation of the magnetic field in the segments. The field is 0.98 T and has a uniformity of 2% over the sample position. The magnets, with their moments aligned are held in a rigid container and rotated under computer control using compressed air. The magnet was designed and made by Magnetic Solutions, Dublin.

The resolution of the experiment is governed by the response of the germanium semiconductor detector, although there are small contributions from the bandwidth of the incident monochromatic beam and the angular acceptance of the detector (the monochromated beam is essentially parallel). The full width at half maximum (FWHM) of the response function in atomic units of momentum can be calculated from the corresponding energy values by using the following equation, which is derived from simple kinematics and relates the photon energies (E_1 incident, E_2 scattered) to the electron momentum, p_z.

$$\frac{p_z}{mc} = \frac{(E_2 - E_1) \pm (E_1 E_2/mc^2)(1 - \cos\phi)}{(E_1^2 + E_2^2 - 2E_1E_2\cos\phi)^{1/2}}. \tag{4}$$

The FWHM of the resolution function at the energy of the Compton peak (67.85 keV) was deduced as 0.48(2) au from measuring the widths of the elastic lines at the three energies 46, 92 and 138 keV.

The reference signals from two additional detectors were recorded in order to monitor the beam intensity, a second Ge solid state detector measured the Compton scattered intensity and a foil-based diode monitored the incident beam directly. The diode monitor was more reliable than the semiconductor detector and its readings were used for normalization of the magnetic effect to the same intensities of the primary beam for the two opposite directions of magnetization of the sample. Although the ring current was very stable, the primary beam extracted from the monochromator sometimes exhibited small, rapid fluctuations. The magnetic field direction was therefore reversed every 30 seconds in order to average the signal. The spectra were saved every 1 hour and inspected for anomalies before being summed. The magnetic effect, M, from which the spin moment per formula unit can be deduced, is defined as

$$M = \frac{I^{\uparrow} - bI^{\downarrow}}{I^{\uparrow} + bI^{\downarrow}} \tag{5}$$

where $I^{\uparrow}$ and $I^{\downarrow}$ represent the integrated Compton intensities for the two (antiparallel) sample magnetization directions, and b is the scaling factor for the beam fluctuations, evaluated from the beam monitor. The correct value of the factor b is confirmed by the disappearance of the elastic line and any parasitic fluorescence lines from the difference (magnetic) profile. The measured magnetic effects of 0.40(1)%, 0.42(1)% and 0.43(1)% were obtained in Cu_2MnAl for [100], [110] and [111] crystallographic directions respectively. This compares with 1.21(1)% for the Fe reference measurement. The total spin moments per formula unit shown in table 1 were determined from these data. The small differences in M with orientation are probably due to different background contribution (e.g. from the sample holder) or the variation in multiple scattering due to the different shape presented by the sample to the beam in the three orientations. These principally affect the total (charge) Compton scattering.

3. Data analysis

The integrated counts for the momentum range -10 au to $+10$ au, which corresponds to energies from 60 to 77 keV, were equal to 7×10^8 under the Compton line in the total (i.e. spin up plus spin down) spectrum and 3×10^6 in the spin-dependent Compton profile (i.e. spin up minus spin down) for the [100] direction. The measurement time was 15 hours. Energy-dependent corrections, namely for absorption in the sample and for the charge and magnetic cross-sections, were applied to the raw data. Since the analysed Compton line lies in a relatively narrow energy range where the efficiency of the Ge detector is close to 100%, no energy-dependent efficiency correction was deemed necessary. Recently it has been shown by Bell *et al* [40] and Honkimäki [46] that the magnetic cross-section itself has a momentum dependence. Fortunately this is linear across the momentum range of the profile and therefore simply averaging the data about $p_z = 0$ effects the correction. The magnetic multiple-scattering contribution was estimated by adapting the Monte Carlo programme originally written for iron [41] for this sample: it was calculated to be less than 5% of the single magnetic scattering and no correction was applied for it. However the multiple charge scattering was much larger and a correction had to be made for it. A number of multiple-scattering simulations of the spectrum of charge scattering were carried out; the optical thickness of the sample was approximately unity for 92 keV radiation and multiple charge scattering amounted to 18.0%, 19.5% and 21% of the single scattering ($\pm 1\%$ in each case) for the [111], [110] and [100] directions, respectively. After correction the total Compton profile was normalized to 44.937 electrons in the range 0–10 au.

At this stage the profiles should approach free atom values at high momenta ($p_z \sim 10$ au) because solid state effects are limited to low momenta, a point that is elaborated upon in section 4 below. Therefore the profiles were compared with a theoretical profile, which had been compiled from tabulated Cu, Mn and Al free atom profiles [42] and convoluted with a Gaussian to mimic the experimental resolution. On the high-energy side of the Compton profile there are parasitic contributions from lead fluorescence (about 2% of the profile area) and a small overlap at high energies with the low-energy side of the Compton line from the 138 keV harmonic of the monochromator. The latter was more difficult to remove and resulted in the data not approaching free atom values in the high-energy tail. Therefore the low-energy side of the line was used in the analysis of the charge profiles. The Compton profiles measured with gamma rays in the laboratory at Bialystok [26] are not subject to these background problems, but suffer from lower statistical precision. The magnetic Compton profiles, which are formed from the difference of two synchrotron measurements, are unaffected by systematic errors of this type and were symmetric about $p_z = 0$.

Finally the magnetic profiles were normalized to a spin moment per formula unit derived with reference to the calibration measurement on iron. The values obtained for the room-temperature moments of Cu_2MnAl were 2.55(7) μ_B for [100], 2.68(7) μ_B for [110] and 2.72(7) μ_B for [111]. The results are prone to systematic errors in the charge scattering, for example in the calculation of the multiple scattering which is larger than normal due to the shape of the crystals (thin plates, which are preferable, were not available). Therefore the value of the saturation magnetization, measured by the magnetic balance technique, of 2.86(5) μ_B, which is assumed to be entirely spin, is preferred for the normalization of the data. It is consistent with the calculated value of 3.4 μ_B at 0 K, given the Curie temperature of 603 K. The values reported here also agree well with the saturation magnetization of Cu_2MnAl published by Bozworth [43] and Dunlap *et al* [44] who found it to be 2.81 μ_B at room temperature. The precise magnetic moments appear to depend upon the thermal history of the individual samples. On the other hand, Oxley *et al* [2] and Endo *et al* [45] quote the value of 3.37 μ_B, which is difficult to reconcile with any of the other published data.

4. Results

4.1. The spin moments on the Mn and Cu sites

The experimental magnetic Compton profiles (all symmetrized by averaging about $p_z = 0$ and normalized to the room-temperature magnetization of 2.86 μ_B) are shown in figure 2, together with those calculated by the KKR CPA method, the latter after convolution with the experimental resolution. The agreement is generally good but the 100 and 111 profiles are lower than predicted for $p_z < 0.7$ au. Since the profiles are normalized to the same area this is compensated by a small excess of experiment over theory for $1 < p_z < 3$ au. The predicted small shoulders representing higher-momentum (umklapp) features in the calculated Compton profile, predicted for $p_z \approx 2.0$ au, are largely smeared out by the resolution and the statistical noise.

The magnetic profiles can be separated into the relative contributions from different atomic sites by using the Compton profiles calculated for electrons in free atoms [42] as basis functions to fit the magnetic line shape. At first sight it might seem unreasonable to use a free atom basis, but it has been shown to be successful in a number of rare earth and actinide ferromagnets [34–36] for the following reason. Free atom momentum densities must provide a good description of the momentum distribution away from the

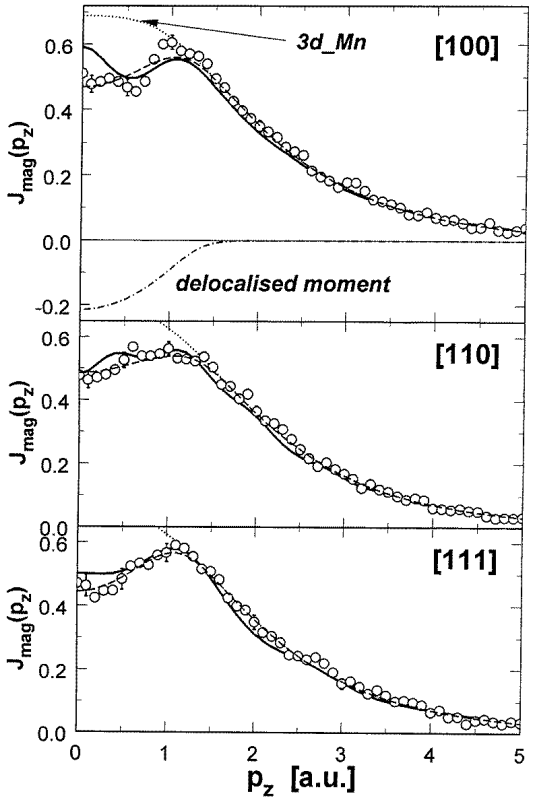

Figure 2. The experimental and theoretical directional spin-dependent (magnetic) Compton profiles of Cu_2MnAl normalized to 2.86 μ_B. The open circles show the experimental data averaged over the low- and high-energy sides of the profile. The statistical errors at low momenta are shown by the error bars; at high momenta these errors are smaller than the diameter of the circles. The solid lines represent the KKR calculations [22] convoluted with a Gaussian of FWHM = 0.5 au to mimic the experimental resolution. Decomposition of the experimental data into the 3d Mn free atom and *free electron* Compton profiles is shown by the dotted and dot–dashed lines respectively (the latter is shown only for the [100] direction). The areas under these profiles are equal to the site-specific spin moments of the sample, i.e. to the localized moment on the Mn site and delocalized moment of sp electrons. The dashed lines represent the sums of the 3d and *free electron* profiles and show the overall quality of the fits to the experimental data. The numerical values for corresponding site spin moments are listed in table 1.

low-momentum region because of the following energy considerations. The second moment of a Compton profile, $\langle p_z^2 J(p_z)\rangle$, or of the parent momentum density, $\langle p^2 n(p)\rangle$, determines the kinetic energy of the system, and hence from the virial theorem, the total energy. Thus the high momentum density is progressively weighted by p^2 in this expression for the energy. On the other hand cohesive energies, which are proportional to the difference between these moments evaluated for the solid and the free atom, are very small fractions of the total energy. Thus, remembering the p^2 weighting, this difference can only derive from significant differences between the free atom's and the solid's Compton profiles for low-momentum behaviour. At higher momenta the density distribution, and therefore the Compton profiles, must be accurately free-atom-like.

The spin-dependent profiles of Cu_2MnAl were fitted by 3d Mn and Cu free atom profiles

and a parabola, which is the profile appropriate to a free electron, to describe the delocalized component. The [100] panel in figure 2 shows all individual profiles in detail, except for the Cu profile which was found to be negligible, as discussed below. The areas under the individual component profiles are equal to the spin magnetic moment on the specific site. The results of the fits are summarized in table 1.

Table 1. Spin moments in Cu_2MnAl. The numbers in parenthesis indicate the error in the last decimal place of the moments, which are quoted in Bohr magnetons.

Orientation	Mn 3d moment (μ_B)	Cu 3d moment (μ_B)	Delocalized moment (μ_B)
100	3.23(2)	$<\|0.05\|$	$-0.37(5)$
110	3.25(2)	$<\|0.05\|$	$-0.39(5)$
111	3.27(2)	$<\|0.05\|$	$-0.41(5)$

The average 3d moment deduced at the Mn site is 3.25(5) μ_B which agrees with the value of 3.21 μ_B obtained by the neutron experiments. The 3d free atom Compton profiles of Cu and Mn are sufficiently similar at the experimental resolution to render the separation of the two components difficult. However by allowing free fits with a number of starting assumptions the spin moment on the copper site was never found to be numerically greater than 0.05 μ_B. This is consistent with neutron results [16] which suggest that the Cu contribution should be negative and no larger, in magnitude, than 0.02 μ_B per formula unit with an error of ± 0.03 μ_B, i.e. essentially zero, but disagrees with the prediction of Ishida *et al* [19].

The central dip at $p_z = 0$ au clearly indicates that the diffuse moment is opposed to the Mn 3d moment. This negative moment, deduced from the three directional measurements, has an average value of 0.39 μ_B. This contradicts the neutron data [16], from which a positive polarization of $+0.17$ μ_B was inferred. The 3d shell of Mn is half full and the polarization of diffuse (itinerant) electrons as a result of p–d hybridization with Al electrons might result in either parallel or antiparallel spin alignments. The experiment shows unequivocally that the delocalized moment assigned to diffuse electrons is antiferromagnetically coupled to the 3d moment at the Mn site. The value of the negative moment per site is $-0.10(2)$ μ_B which is in reasonable agreement with the prediction of Ishida *et al* [19].

4.2. The sphericity of the spin density

According to the neutron data the anisotropy of position space magnetization density, which is assumed to be the spin magnetization density, should be small; the same should also be true of the magnetic Compton profiles. The neutron results were consistent with a form factor based on a spherical spin density for the Mn^{2+} ion [20]. As shown in figure 3 the differences between the directional magnetic Compton profiles are significant, but only just above the level of statistical errors. The dashed lines are drawn through the experimental points to guide the eye and illustrate that there are some deviations from sphericity at low momenta, which in general follow the indications of theory (solid line). Inspection of the individual profiles shows that the largest differences at low momentum originate from the differences between experiment and theory for the [100] magnetic Compton profile (see figure 2).

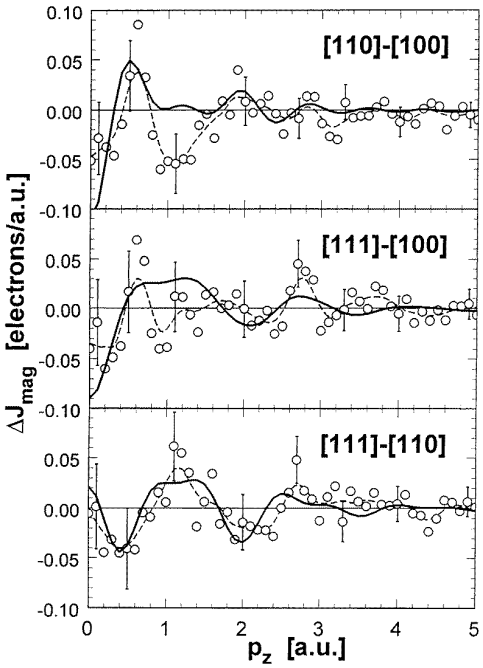

Figure 3. Difference profiles reflecting the anisotropies in directional magnetic profiles of Cu_2MnAl. The experimental and theoretical differences are plotted by the open circles and the solid lines respectively. The latter were obtained from the theoretical KKR data convoluted with a Gaussian of FWHM = 0.5 au. The dashed curves are drawn through the data as a guide to the eye. They illustrate the fact that there are anisotropies at low momenta, which are statistically significant and are similar to the predictions of theory.

4.3. Asphericity of the charge density and the majority and minority bands

Figure 4 shows the anisotropies of the Compton profiles, $J(p_z)$, of Cu_2MnAl formed by the differences between pairs of directional charge profiles. The upper set are theoretical and show some differences, especially close to $p_z = 0$, between the new KKR calculation [22] for the ferromagnetic ground state and the previous model which started from a paramagnetic ground state. The oscillations are predicted to be similar in their period because those features derive from the geometry of the Brillouin zone. On the other hand the amplitudes differ due to the difference in the description of the electron wavefunctions. In the lower set they are compared with experiment (the gamma ray data are used for the reasons explained previously) and it is clear that the ferromagnetic ground state calculation is superior. The only significant disagreement between experiment and theory lies in the scale of the anisotropies. The overestimation of these directional differences is a familiar result in studies of the elemental transition metals (see [23]) and is ascribed to the failure of the local density approximation to describe electron–electron correlations adequately.

The majority and minority band profile differences, $J(p_z)\uparrow$ and $J(p_z)\downarrow$ were calculated from the total and magnetic Compton profiles. Referring back to equations (1) and (2) it is easy to see that:

$$J(p_z)\uparrow = \tfrac{1}{2}[J(p_z) + J_{mag}(p_z)]$$
$$J(p_z)\downarrow = \tfrac{1}{2}[J(p_z) - J_{mag}(p_z)]. \qquad (6)$$

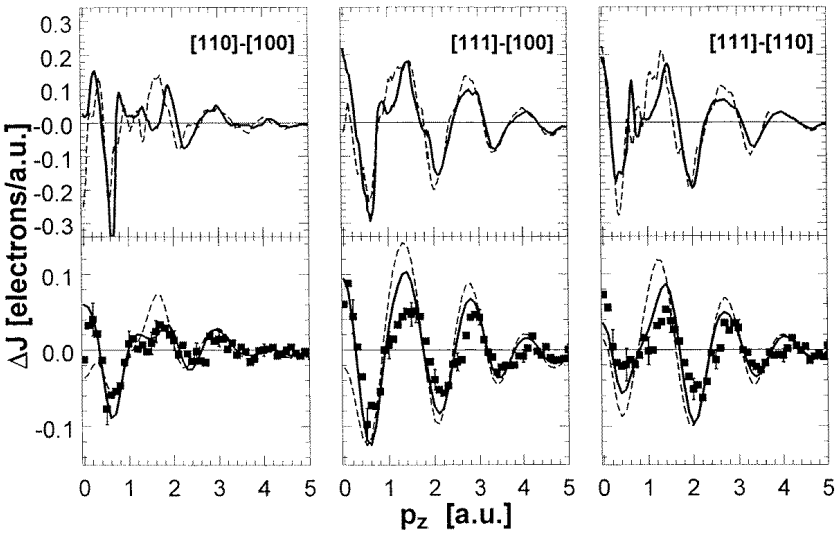

Figure 4. The directional anisotropies of the total (i.e. charge scattering) Compton profiles of Cu_2MnAl. The upper plots represent the theoretical predictions calculated for ferromagnetic (the solid lines) and paramagnetic (the dashed lines) ground states. The lower plots show the experimental results from directional Compton measurements made with a gamma spectrometer using photons of incident energy 661.6 keV (the solid rectangles), compared with the same theoretical KKR profiles now convoluted with a Gaussian to mimic the experimental resolution. The theory which starts from a ferromagnetic ground state (solid lines) provides a superior description of the anisotropy of the charge density.

These quantities are prone to systematic errors because the errors contributing to the charge and magnetic profile are different and will not necessarily disappear even when the difference is taken (e.g. for the minority profile). The systematic errors are removed by considering the directional differences between these quantities and this is what has been done here. The theoretical and experimental band-dependent differences are shown in figure 5, the theoretical predictions being shown by the solid lines. The two sets of experimental data combined to give these curves are the magnetic Compton profiles obtained in the synchrotron experiment and the charge profiles obtained in the same measurement (open triangles) and in the gamma ray study (filled circles). The latter have slightly better resolution than the former, as is evident from the slightly greater pitch of the oscillations, but the difference is not too large to invalidate their combination. The gamma ray data do however have poorer statistical accuracy as is evident from their larger scatter. The solid line is the KKR prediction. The overall agreement of the experimental and theoretical data is good. There are significant anisotropies in both majority and minority band Compton profiles. There is no simple relationship between the anisotropy of these spin-resolved bands, which include all the electrons, and the density of states representation in which the minority 3d orbitals on Mn were predicted to be unoccupied [10, 11].

5. Conclusions

The diffuse conduction electron contribution to the spin moment ($-0.4\ \mu_B$) is coupled antiferromagnetically to the 3d moment in contradiction to neutron data which reported a

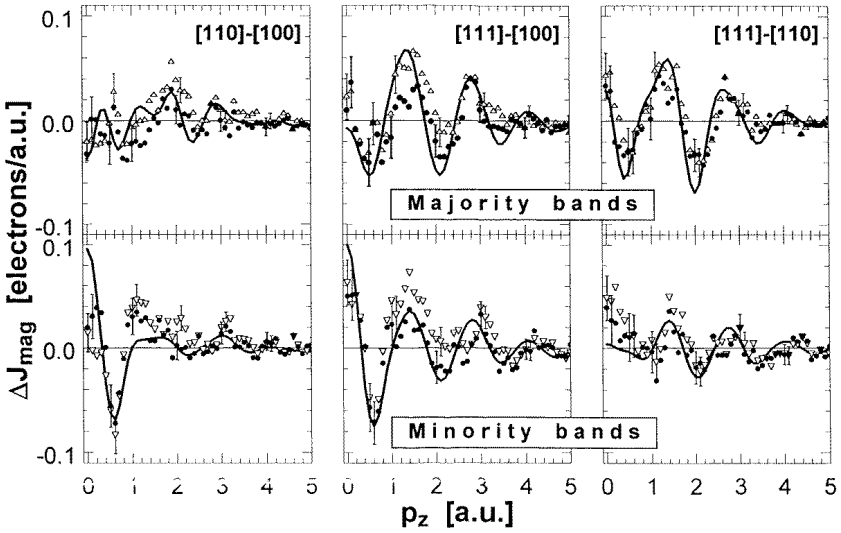

Figure 5. The anisotropies of majority and minority electron band Compton profiles of Cu_2MnAl are shown in the upper and lower set of graphs respectively. The sums of top and bottom curves of each pair give the anisotropies in the total Compton profiles shown in figure 4 whereas their differences are the anisotropies of the spin-dependent profiles shown in figure 3. The experimental data, combined from both the high-energy gamma measurements ($E = 661.6$ keV) and the synchrotron study ($E = 92$ keV) are plotted by the filled circles and empty triangles respectively. The solid lines show the theoretical differences obtained from the KKR data convoluted with a Gaussian of FWHM = 0.5 au.

parallel moment of $+0.17\ \mu_B$. On the other hand the 3d spin moment of $3.25\ \mu_B$ on the Mn site is in agreement with neutron data and is well reproduced by its 3d atomic Compton profile at momenta above 1.5 au. Our results are in agreement with new KKR calculations. Also within statistical accuracy ($\pm 0.05\ \mu_B$) there is no magnetic contribution from the Cu site, again in agreement with neutron data. The spin density distribution is almost spherical, with the asphericities at low momentum just statistically significant and in qualitative agreement with band theory. The experiment confirms that the momentum densities in both majority and minority bands are strongly anisotropic. The comparison between experiment and theory also underlines the importance of performing the calculations using a ferromagnetic ground state.

Acknowledgments

We are grateful to the ESRF for allocating beamtime for this experiment and to V Honkimäki, J McCarthy and P Suortti and other beamline staff at ESRF for active support and advice during the measurements. Special thanks are due to K Perzynska and M Biernacka for saturation magnetization measurements. This work was part of a research programme supported by the EPSRC in the UK, the Committee for Scientific Research (KBN grant No 2P03B06108) in Poland and the EU Human Capital and Mobility Initiative (contract ERB CHR/XTC/930135).

References

[1] *Landolt–Börnstein 1988 New Series* vol 19c (Berlin: Springer) pp 75–185
[2] Oxley D P, Tebble R S and Williams K C 1963 *J. Appl. Phys.* **34** 1362
[3] Kozubski R and Soltys J 1982 *J. Mater. Sci.* **17** 1441
[4] Soltys J, Stefaniak M and Holender J 1984 *Phil. Mag.* B **49** 151
[5] Sakka Y and Nakamura M 1990 *J. Mater. Sci.* **25** 2549
[6] Robinson J S, McCormick P G and Street R 1995 *J. Phys.: Condens. Matter* **7** 4259
[7] Noda Y and Ishikawa Y 1976 *J. Phys. Soc. Japan* **40** 699
[8] Ishikawa Y 1977 *Physica* B **91** 130
[9] Tajima K, Ishikawa Y, Webster P J, Stringfellow M W, Tocchetti D and Ziebeck K R A 1977 *J. Phys. Soc. Japan* **43** 483
[10] Williams A R, Moruzzi V L, Gelatt C D Jr and Kübler J 1983 *J. Magn. Magn. Mater.* **31–34** 88
[11] Kübler J, Williams A R and Sommers C B 1983 *Phys. Rev.* B **28** 1745
[12] Kübler J 1984 *Physica* B **27** 257
[13] Fujii S, Sugimura S, Ishida S and Asano S 1990 *J. Phys.: Condens. Matter* **2** 8583
[14] Tobola J, Pierre J, Kaprzyk S,. Skolozdra RV and Kouacou M A 1996 *J. Magn. Magn. Mater.* **159** 192
[15] Brown D, Crapper M D, Bedwell K H, Flannery L B, Petty M and Skull P A 1996 *J. Phys.: Condens. Matter* **8** 5941
[16] Rakhecha V C, Chakravarthy R and Satya Murthy N S 1976 *Proc. Conf. on Neutron Scattering (Gatlinburg, TN, 1976)* vol 2, p 638
[17] Forsyth J B 1963 *Acta Crystallogr. Suppl.* **16** A126
[18] Takata H 1965 *J. Phys. Soc. Japan* **20** 1743
[19] Ishida S, Kubo Y, Ishida J and Asano S 1980 *J. Phys. Soc. Japan* **48** 814
[20] Watson R E and Freeman A J 1961 *Acta Crystallogr.* **14** 231
[21] Ishikawa Y, Tajima K and Radakrishna P 1976 *J. Phys. Soc. Japan* **40** 1597
[22] Kaprzyk S 1997 *Acta Phys. Pol.* A **91** 135
[23] Cooper M J 1985 *Rep. Prog. Phys.* **218** 415
[24] Lovesey S W 1996 *J. Phys.: Condens. Matter* **8** L353
[25] Sakai N 1996 *J. Appl. Crystallogr.* **29** 81
[26] Andrejczuk A, Zukowski E, Dobrzynski L, Neumann K-U and Ziebeck K R A 1997 *Nukleonika* **42** 5
[27] Sakai N and Ôno K 1976 *Phys. Rev. Lett.* **37** 351
[28] Cooper M J, Laundy D, Cardwell D A, Timms D N, Holt R S and Clark G 1986 *Phys. Rev.* B **34** 5984
[29] Cooper M J, Zukowski E, Collins S P, Timms D N, Itoh F and Sakurai H 1992 *J. Phys.: Condens. Matter* **4** L399
[30] Timms D N, Zukowski E, Cooper M J, Laundy D N, Collins S P, Itoh F, Sakurai H, Iwazumi T, Kawata H, Ito M, Sakai N and Tanaka Y 1993 *J. Phys. Soc. Japan* **62** 1716
[31] Sakai N 1994 *J. Phys. Soc. Japan* **63** 4655
[32] Carra P, Fabrizio M, Santoro G and Thole B T 1996 *Phys. Rev.* B **53** R5994
[33] Sakai N 1992 *Mater. Sci. Forum* **105–110** 431
[34] Zukowski E, Collins S P, Cooper M J, Timms D N, Itoh F, Sakurai H, Kawata H, Tanaka Y and Malinowski A 1993 *J. Phys.: Condens. Matter* **5** 4077
[35] Cooper M J, Lawson P K, Dixon M A G, Zukowski E, Timms D N, Itoh F, Sakurai H, Kawata H, Tanaka Y and Ito M 1996 *Phys. Rev.* B **54** 4068
[36] Lawson P K, Cooper M J, Dixon M A G, Timms D N, Zukowski E, Itoh F and Sakurai H 1997 *Phys. Rev.* B **56** 3239
[37] Sakai N, Koizumi A, Miyamoto N and Tanaka Y 1997 *AIP 1997 Conf. Proc.* 399
[38] McCarthy J E, Cooper M J, Lawson P K, Timms D N, Manninen S O, Hämäläinen K and Suortti P 1997 *J. Synchrotron. Radiat.* **4** 102
[39] Holt R S and Cooper M J 1983 *Nucl. Instrum. Methods* **213** 447
[40] Bell F, Felsteiner J and Pitaevskii L P 1996 *Phys. Rev.* A **53** R1213
[41] Sakai N 1987 *J. Phys. Soc. Japan* **56** 2477
[42] Biggs F, Mendelsohn L B and Mann J B 1975 *At. Nucl. Data Tables* **16** 201
[43] Bozworth R M 1951 *Ferromagnetism* (New York: van Nostrand)
[44] Dunlap R A, Stroink G and Dini K 1986 *J. Phys. F: Met. Phys.* **16** 1083
[45] Endo K, Phayama T and Kitamura R 1964 *J. Phys. Soc. Japan* **19** 1494
[46] Honkimäki V 1997 Private communication